Korean J. Chem. Eng., 38(9), 1826-1833 (2021)
DOI: 10.1007/s11814-021-0861-x

pISSN: 0256-1115
eISSN: 1975-7220

Effects of Pluronic P123 addition and Cr^{3+} doping on electrochemical properties of $Li_4Ti_5O_{12}$ anode for lithium ion batteries

Jin-Seong Seo and Byung-Ki Na†

Department of Chemical Engineering, Chungbuk National University,
1 Chungdae-ro, Seowon-gu, Cheongju, Chungbuk 28644, Korea
(*Received 31 January 2021 • Revised 10 May 2021 • Accepted 2 June 2021*)

Abstract−Spinel $Li_4Ti_5O_{12}$ is an attractive anode material for lithium ion batteries due to its stable electrochemical characteristics. However, its low electrical conductivity is regarded as a critical disadvantage for commercialization. The addition of P123 with Cr^{3+} doping enhanced the surface area and the electrical conductivity, which improved the electrochemical properties of $Li_4Ti_5O_{12}$. As-prepared samples were analyzed by X-ray diffraction, X-ray photoelectron spectroscopy, field-emission scanning electron microscopy, as well as BET and BJH analysis. Electrochemical properties were investigated by cyclic voltammetry, electrochemical impedance spectroscopy, powder conductivity measurement and cycle performance testing. P-$Li_4Ti_{4.95}Cr_{0.05}O_{12}$ showed excellent rate performance of 191, 189, 184, 175, 157, and 137 mAh/g at C-rates of 0.2, 0.5, 1, 2, 5, and 10 and high stable capacity retention of 147 mAh/g at a C-rate of 10 after 300 cycles.

Keywords: Lithium-ion Battery, $Li_4Ti_5O_{12}$, Doping, Electrical Conductivity, Porous Materials, P123

INTRODUCTION

Since lithium titanium oxide with lithium intercalation properties was first reported by Murphy in 1983, the spinel-structure $Li_4Ti_5O_{12}$ anode material has attracted much attention as a next-generation anode material for lithium ion batteries [1,2]. $Li_4Ti_5O_{12}$ has a zero-strain with little volume change when lithium is intercalated/deintercalated and it has highly stable surface characteristics. Formation of a solid electrolyte interface (SEI) layer on the $Li_4Ti_5O_{12}$ surface rarely occurs due to its high operating potential (1.55 V) in comparison to that of SEI layer formation potential (Li^+/Li vs below 1 V) [3,4].

However, due to its low electrical conductivity (~10^{-13} S/cm) $Li_4Ti_5O_{12}$ has poor capacity retention at high current density [5]. To solve this problem, researchers have suggested a variety of methods. The first method is carbon coating on the $Li_4Ti_5O_{12}$ surface. When a carbon material with high electrical conductivity is coated on the $Li_4Ti_5O_{12}$ surface, lithium ion diffusion occurs easily to $Li_4Ti_5O_{12}$ surface. Capacity retention can be enhanced at high current density [6,7]. The second method is transition metal doping on titanium or lithium sites. When M^+ ions (Tb [8], Mn [9], Zr [10], Ni [11], Mg [12], etc.) are doped at Ti^{4+} sites, $Li_4Ti_5O_{12}$ shows semiconducting characteristics. Thus, the electrical conductivity and diffusion coefficient can be improved. The third method is reducing the particle size of $Li_4Ti_5O_{12}$ or modification of its morphology or porous structure, which can shorten the lithium ion pathway [13]. A porous structure helps the diffusion of lithium ions inside $Li_4Ti_5O_{12}$ particles [14].

Pluronic P123 is known to prevent particle agglomeration, and it functions as a pore-forming agent in wet-chemical synthesis. Because small particle size and pores within particles ease the diffusion of lithium ions into crystalline $Li_4Ti_5O_{12}$, the electrochemical characteristics of $Li_4Ti_5O_{12}$ can be improved [15].

In this study, the synergistic effects of Pluronic P123 addition and Cr^{3+} doping on the physical and electrochemical characteristics of $Li_4Ti_5O_{12}$ were investigated. Pluronic P123 was used as a dispersant and pore-forming agent. When Cr^{3+} was doped into the Ti^{4+} position, the semi-conducting characteristics improved the lithium ion diffusion coefficient and electrical conductivity. The Cr^{3+} 3d band is close to the Ti^{4+} 3d bands and no gap between Cr^{3+} 3d bands and Ti^{4+} 3d bands. So, the electrons in Cr^{3+} 3d bands can be easily moved to Ti^{4+} bands for Cr^{3+} doped $Li_4Ti_5O_{12}$. The electrical conductivity of Cr^{3+} doped $Li_4Ti_5O_{12}$ can be enhanced. Band gap of Fe^{3+} doped $Li_4Ti_5O_{12}$ is calculated as 0.7 eV, so the electrons in Fe^{3+} doped $Li_4Ti_5O_{12}$ are hard to move from Fe^{3+} 3d bands to Ti^{4+} 3d bands. Ni^{2+} doped $Li_4Ti_5O_{12}$ is also hard to excite electrons from Ni^{2+} 3d bands to Ti^{4+} 3d bands because Ni^{2+} 3d band is localized [16]. Doping causes the formation of stable and thin SEI film, which lowers the resistance of SEI layer and allows the easy movement of lithium ions during the charge/discharge process. Therefore, electrochemical properties of P-Li4$Ti_{5-x}Cr_xO_{12}$ can be improved [17].

Cr^{3+} can be easily doped into the Ti^{4+} position, and electron transport can be improved. Experiments were conducted by varying the doping ratios of Ti^{4+} : Cr^{3+} to 4.97 : 0.03, 4.95 : 0.05 and 4.93 : 0.07, and the samples were named as P-$Li_4Ti_{4.97}Cr_{0.03}O_{12}$, P-$Li_4Ti_{4.95}Cr_{0.05}O_{12}$, and P-$Li_4Ti_{4.93}Cr_{0.07}O_{12}$, respectively.

EXPERIMENTAL

1. Synthesis of Cr^{3+} Doped Porous $Li_4Ti_5O_{12}$

Samples produced with Pluronic P123 addition and Cr^{3+} doping were synthesized by the evaporation-induced self-assembly (EISA)

†To whom correspondence should be addressed.
E-mail: nabk@chungbuk.ac.kr

method. In beaker 1, 1.5 g of P123 was put into 50 ml of distilled water and stirred until the P123 was completely dissolved. In beaker 2, $LiNO_3$ (Sigma-Aldrich, 98%), titanium (IV) butoxide (Sigma-Aldrich, 97%), and $Cr(NO_3)_3{\cdot}9H_2O$ were added to 20 ml of ethanol and stirred for 2 hours.

The solution in beaker 2 was added dropwise into beaker 1, and the mixture was stirred for 3 hours at 70 °C. The solution was evaporated in a heating mantle at 70 °C for 24 h and dried completely at 150 °C for 24 h. The dried sample was calcined at 750 °C for 12 h under an oxygen atmosphere. It was heated from 25 °C to 700 °C at a heating rate of 5 °C/min and from 700 °C to 750 °C at a rate of 1 °C/min. Porous structured $Li_4Ti_{5-x}Cr_xO_{12}$ ($0.03 \le x \le 0.07$) was synthesized to identify the electrochemical effect of Cr^{3+} doping.

2. Materials Characteristics

The crystal structure of the as-prepared samples was investigated by X-ray diffraction analysis (XRD, Bruker ASX). Changes in the binding energies due to Cr^{3+} doping were examined by X-ray photoelectron spectroscopy (XPS, Ulvac-PHI, PHI Quantera-II). Particle morphologies and particle sizes of pure-$Li_4Ti_5O_{12}$, P-$Li_4Ti_5O_{12}$, and P-$Li_4Ti_{5-x}Cr_xO_{12}$ were investigated by field-emission scanning electron microscopy (FE-SEM, CrossBeam 540, ZEISS). The BET (Brunauer-Emmett-Teller) surface area and BJH (Barrett-Joyner-Halenda) pore-size distribution were measured by using a surface area analyzer (Micromeritics, ASAP 2420). Electrical conductivity in accordance with Cr^{3+} doping was estimated by powder resistance analysis (Han tech, HPRM-M2).

3. Electrochemical Characteristics

The electrochemical characteristics were tested with half-cells. Slurry for an electrode was produced with the ratio of active material : conductor : binder to be 80 : 10 : 10 (wt.%). Acetylene black was used as a conductor, and polyvinylidene fluoride (PVdF, Solef5130, Solvay Korea) [8% in 1-methyl-2-pyrrolinone (NMP, Sigma-Aldrich)] was used as a binder. NMP was also used to control the viscosity of the slurry. The as-prepared slurry was coated on Cu-foil with a 50-μm-thick doctor blade. The coated electrode was dried in an oven at 80 °C for 12 h to evaporate the moisture and solvent.

CR2032 coin cells were assembled in a globe box filled with argon gas, and lithium metal was used as a counter electrode. A 20-μm poly-ethylene membrane (W-scope Korea, COD 20A) was used to separate the cathode and anode, and 1.15 M $LiPF_6$ in a 3 : 7 (v/v) mixture of ethylene carbonate (EC) : ethyl-methyl carbonate (EMC) (Panax E-tec) was used as an electrolyte.

The rate and cycling performance of CR2032 half cells were investigated with cycle tester (WBS-3000L, Won-A tech) under a cut-off voltage range of 1.0 to 2.5 V at various charge/discharge rates. After the cycle performance test, electrochemical impedance spectroscopy analysis (ZIVE-MP1, Won-A Tech) was conducted to measure the resistance characteristics in a range from 0.1 to 10,000 Hz. Cyclic voltammetry (CV) (ZIVE-MP1, Won-A Tech) was conducted with operating voltages from 1.0 to 2.5 V and scan rates from 0.1 to 5 mV/s.

RESULTS AND DISCUSSION

The effect of porous structure and Cr^{3+} doping to increase the electrical conductivity, lithium ion diffusion, and electrochemical characteristics of $Li_4Ti_5O_{12}$ was tested. Crystalline structure of pure-$Li_4Ti_5O_{12}$ and P-$Li_4Ti_{5-x}Cr_xO_{12}$ was investigated by XRD, and the results are shown in Fig. 1. The XRD result of the (111) plane is shown in Fig. 1(b). The ionic radius of Cr^{3+} is 0.062 nm and that of Ti^{4+} is 0.068 nm [18,19].

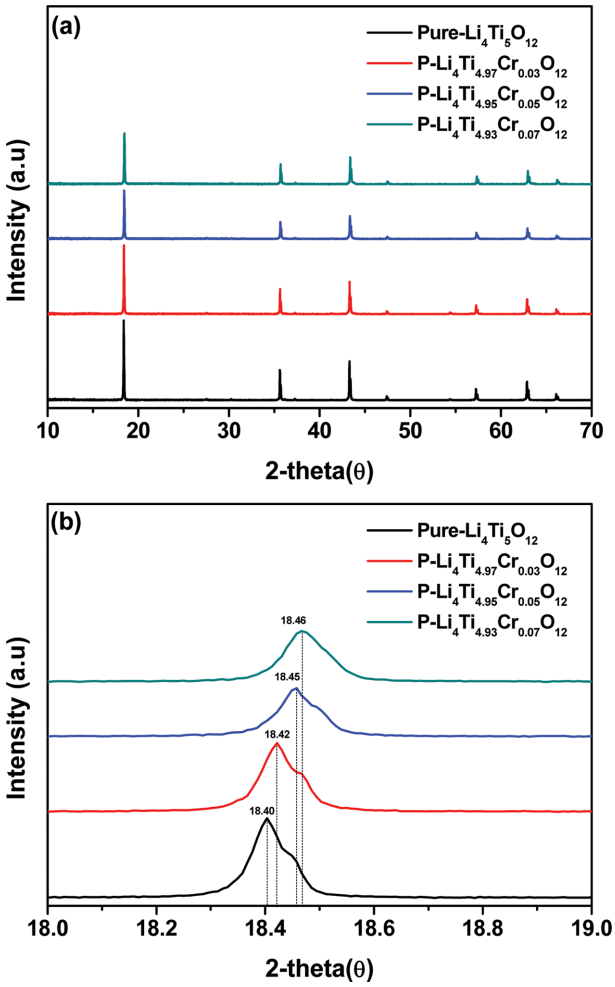

Fig. 1. XRD peaks of (a) pure $Li_4Ti_5O_{12}$ and P-$Li_4Ti_{5-x}Cr_xO_{12}$ ($0 \le x \le 0.07$) and (b) enlarged peaks at (111) plane.

Small Cr^{3+} is more likely to be doped into the relatively large Ti^{4+} position. Ti^{4+} is partially reduced to Ti^{3+}, and oxygen vacancies are produced. These oxygen vacancies increase the electron concentration, and electrical conductivity can be increased [20]. As the Cr^{3+} doping level is increased, 2-theta of XRD peaks are increased. This means that doping of Cr^{3+} into the Ti^{4+} position decreases the lattice parameters.

The lattice parameters of all samples were calculated, and the values are shown in Table 1. The lattice parameters of $Li_4Ti_5O_{12}$ decreased from 8.3593 Å (pure-$Li_4Ti_5O_{12}$) to 8.3159 Å (P-$Li_4Ti_{4.93}Cr_{0.07}O_{12}$) as the amount of Cr^{3+} doping increased. When small radius Cr^{3+} was doped into the large radius Ti^{4+} position, the lattice parameter decreased. This narrowed the lithium ion pathway and degraded the electrochemical characteristics [21]. Therefore, it is important to choose a proper doping level to minimize the decrease of the lattice parameter [22].

Table 1. Lattice parameters of pure $Li_4Ti_5O_{12}$ and P-$Li_4Ti_{5-x}Cr_xO_{12}$ at (111) plane

Samples	Lattice parameter (Å)
Pure-$Li_4Ti_5O_{12}$	8.3593
P-$Li_4Ti_{4.97}Cr_{0.03}O_{12}$	8.3480
P-$Li_4Ti_{4.95}Cr_{0.05}O_{12}$	8.3272
P-$Li_4Ti_{4.93}Cr_{0.07}O_{12}$	8.3159

Table 2. Crystalline size of pure-$Li_4Ti_5O_{12}$ and P-$Li_4Ti_{5-x}Cr_xO_{12}$ at (111) plane calculated by Scherrer equation

Samples	Crystalline size
Pure-$Li_4Ti_5O_{12}$	105.4 nm
P-$Li_4Ti_{4.97}Cr_{0.03}O_{12}$	94.7 nm
P-$Li_4Ti_{4.95}Cr_{0.05}O_{12}$	91.4 nm
P-$Li_4Ti_{4.93}Cr_{0.07}O_{12}$	89.8 nm

The crystalline sizes were calculated by the Scherrer Eq. (1) at the (111) plane:

$$t = \frac{K\lambda}{\beta\cos\theta} \quad (1)$$

where t is the crystalline size of $Li_4Ti_5O_{12}$, K is the shape value (generally 0.9), λ is the x-ray wavelength (0.15406 nm), β is the width of the peak at half maximum height, and θ is the x-ray incident angle.

Table 2 shows the crystalline size of $Li_4Ti_5O_{12}$ in accordance with Cr^{3+} doping level. Small crystalline size shortens the diffusion pathway of lithium ions, so they can easily diffuse inside the $Li_4Ti_5O_{12}$ matrix [23]. Surface diffusion can be improved due to the large contact area between the $Li_4Ti_5O_{12}$ surface and the electrolyte [24].

Fig. 2 shows FE-SEM images of $Li_4Ti_5O_{12}$ in accordance with P123 addition and Cr^{3+} doping. Fig. 2(a) is an FE-SEM image of pure-$Li_4Ti_5O_{12}$, and Fig. 2(b) is that of P-$Li_4Ti_5O_{12}$. The particle size

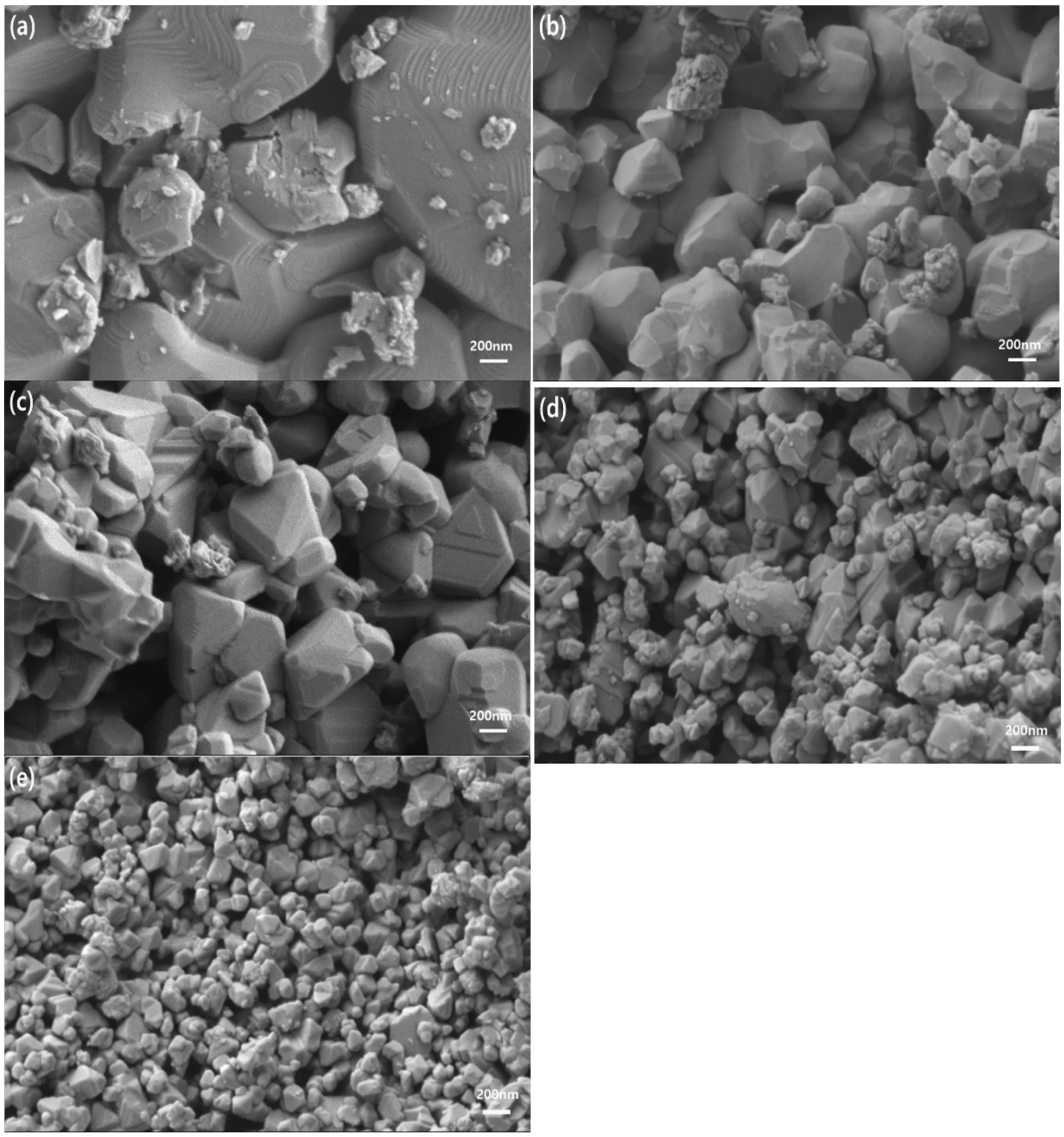

Fig. 2. FE-SEM Images of (a) pure-$Li_4Ti_5O_{12}$, (b) P-$Li_4Ti_5O_{12}$, (c) P-$Li_4Ti_{4.93}Cr_{0.07}O_{12}$, (d) P-$Li_4Ti_{4.95}Cr_{0.05}O_{12}$, and (e) P-$Li_4Ti_{4.93}Cr_{0.07}O_{12}$.

of P-$Li_4Ti_5O_{12}$ is smaller than that of pure-$Li_4Ti_5O_{12}$. This means that the addition of P123 helps decrease of particle size and acts as a dispersant to prevent the agglomeration of particles. Moreover, Cr^{3+} doping plays a role in reducing the particle. When the Cr^{3+} doping level increased, particle size tended to gradually decrease. The result of reducing particle size through transition metal ion doping has been previously demonstrated [25-27].

The specific surface area and pore-size distribution were measured by the Brunauer-Emmett-Teller (BET) and Barrett-Joyner-Halenda (BJH) methods. The BET surface areas of pure-$Li_4Ti_5O_{12}$, P-$Li_4Ti_5O_{12}$, and P-$Li_4Ti_{4.95}Cr_{0.05}O_{12}$ were 0.98, 3.2, and 6.9 m^2/g, respectively. The average pore diameters of P-$Li_4Ti_5O_{12}$ and P-$Li_4Ti_{4.95}Cr_{0.05}O_{12}$ were 2 to 3 nm, but pure-$Li_4Ti_5O_{12}$ has no pores. P123 forms micelles as the solvent is evaporated. PEO chains of P123 are weakly bonded with titanium ions (e.g., hydrogen bonding, van der Waals force), so titanium ions can be dispersed by P123 micelles, which can prevent particle agglomeration. During heat-treatment, P123 is removed and pores are formed at the sites of P123 [28].

Particle size is reduced through the synergic effects of P123 addition and Cr^{3+} doping. As the particle size becomes smaller, the diffusion pathway of lithium ions becomes shorter, and contacting area between electrolytes and the $Li_4Ti_5O_{12}$ surface is increased [29,30].

When Cr^{3+} is doped into the Ti^{4+} position of the $Li_4Ti_5O_{12}$ host lattice, Ti^{4+} ions are partially reduced to Ti^{3+}. Partially reduced Ti^{4+} is known to contribute to improving electrochemical properties by increasing electron concentration [31].

To investigate the effect of Cr^{3+} doping, XPS analysis was conducted. The XPS results of pure-$Li_4Ti_5O_{12}$ and P-$Li_4Ti_{4.95}Cr_{0.05}O_{12}$ are shown in Fig. 3. The Ti^{4+} $2p_{3/2}$ peak of pure-$Li_4Ti_5O_{12}$ appeared at 459.1 eV, while that of P-$Li_4Ti_{4.95}Cr_{0.05}O_{12}$ appeared at 458.7 eV. The peak shifting of 0.4 eV means that Ti^{4+} was partially reduced by Cr^{3+} doping, and Ti^{3+} was formed.

The XPS spectra were fitted for further analysis. The weak Ti^{3+} peak of P-$Li_4Ti_{4.95}Cr_{0.05}O_{12}$ appeared at 457.3 eV as shown in Fig. 3(b). The result indicates that surface Ti^{4+} is reduced to Ti^{3+} by Cr^{3+} doping. Electrical conductivity can be enhanced due to oxygen vacancies, free electrons by Cr^{3+} doping [10,32]. Powder resistance analysis was conducted to measure the electrical conductivity of pure-$Li_4Ti_5O_{12}$ and P-$Li_4Ti_{5-x}Cr_xO_{12}$. The applied pressure ranged from 25 to 200 MPa. The electrical resistance of powders is associated with the contact area between particles. As the pressure increases, the contact area is increased, and the resistance is reduced [33]. Electrons in Cr^{3+} bands can be easily excited to Ti^{4+} 3d bands because there is no band gap between Cr^{3+} 3d bands and Ti^{4+} 3d bands. Therefore, the electrical conductivity of $Li_4Ti_5O_{12}$ can be increased by Cr^{3+} doping [16].

Fig. 4 shows the electrical conductivities of the powder samples. When Cr^{3+} was doped, the electrical conductivity increased gradually. The electrical conductivity also increased as the pressure was increased. The electrical conductivity increased because of doping of Cr^{3+} into the octahedral 16d site of Ti^{4+}. Thus, electron holes and free electrons were formed. Ceramics tend to maintain electron neutrality. As $Li_4Ti_5O_{12}$ is partially reduced to Ti^{3+} by Cr^{3+} doping, the electron concentration is increased to meet electron neutrality and the electrical conductivity increases. In other cases, when Cr^{3+} is doped into Li^+ position, free electrons can be created by higher Cr^{3+}

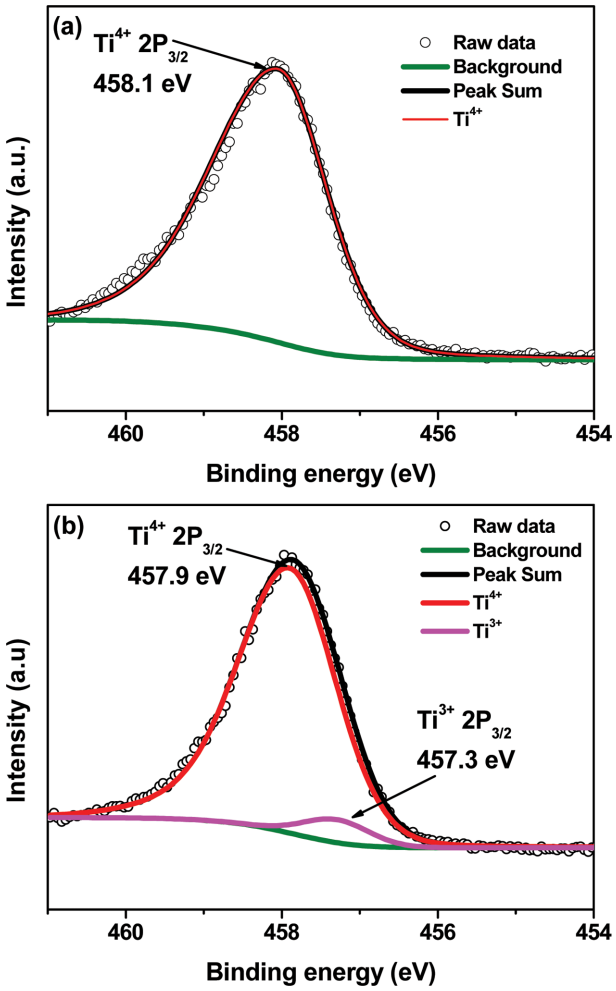

Fig. 3. XPS spectra of Ti^{4+} $2p_{3/2}$ in (a) pure-$Li_4Ti_5O_{12}$ and (b) P-$Li_4Ti_{4.95}Cr_{0.05}O_{12}$.

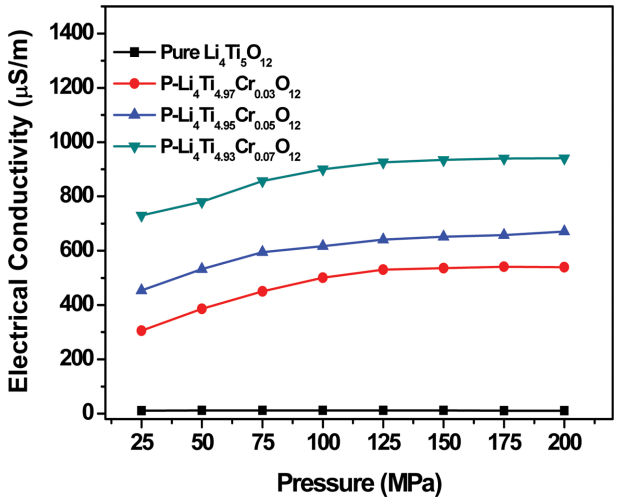

Fig. 4. Electrical conductivities of pure-$Li_4Ti_5O_{12}$ and P-$Li_4Ti_{5-x}Cr_xO_{12}$ ($0 \le x \le 0.07$) obtained from powder conductivity measurement with the pressure from 25 to 200 MPa.

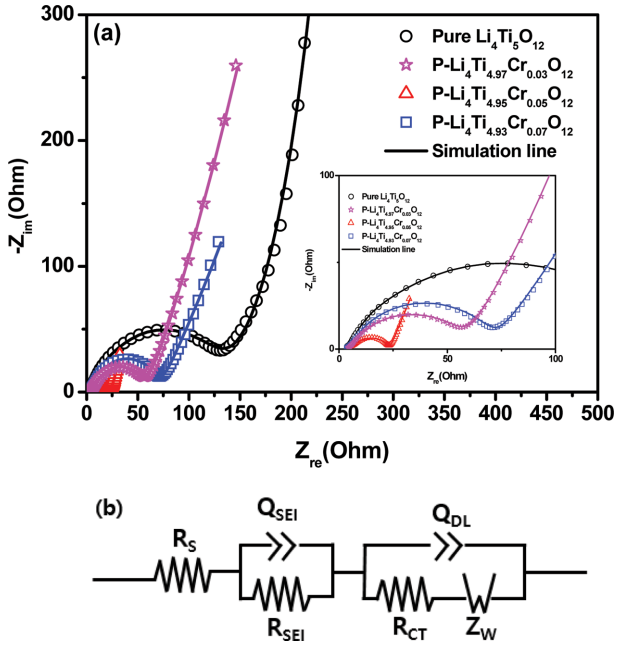

Fig. 5. (a) Nyquist plots of pure-$Li_4Ti_5O_{12}$ and P-$Li_4Ti_{5-x}Cr_xO_{12}$ (0≤ ≤0.07) obtained after rate performance test with the frequency from 1 to 100 KHz and (b) the equivalent circuit model.

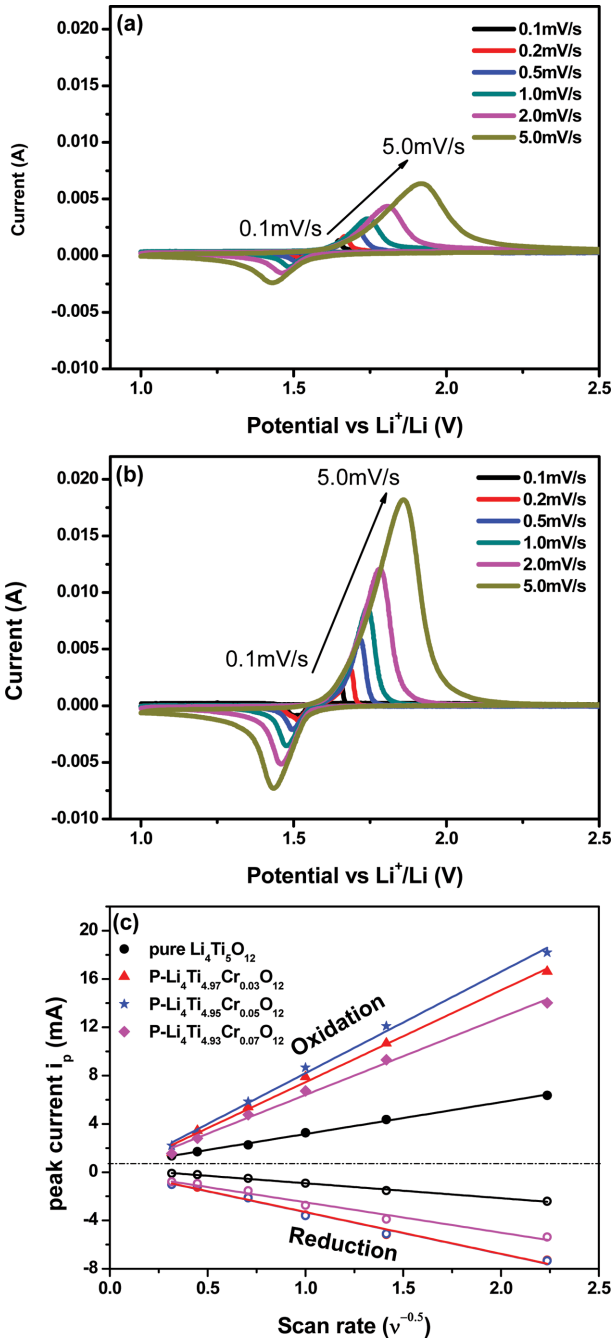

Fig. 6. Cyclic voltammetric results of (a) pure-$Li_4Ti_5O_{12}$, (b) P-$Li_4Ti_{4.95}Cr_{0.05}O_{12}$ with the scan rate from 0.1 to 5 mV/s, and (c) the relationship between the scan rate ($v^{-0.5}$) and the peak current i_p (mA) of pure-$Li_4Ti_5O_{12}$ and P-$Li_4Ti_{5-x}Cr_xO_{12}$ (0≤x≤0.07).

electrovalence and the electrical conductivity increases [34]. Improvement of electrical conductivity by Cr^{3+} doping can be expected to reduce the charge-transfer resistance and to enhance the rate capability of P-$Li_4Ti_{5-x}Cr_xO_{12}$ [35].

Electrochemical impedance spectroscopy (EIS) analysis was conducted to analyze the resistance characteristics of $Li_4Ti_5O_{12}$ with Cr^{3+} doping. The EIS results for pure-$Li_4Ti_5O_{12}$ and P-$Li_4Ti_{5-x}Cr_xO_{12}$ anode materials are shown in Fig. 5(a) and (b). Impedance measurements were conducted after cycle performance testing of the samples. The Nyquist plots were fitted by Z-MAN software. According to the Nyquist plots, all samples showed similar Nyquist circles. Resistances at high frequency are solution resistance (R_S), and those at medium frequency are solid electrolyte interface resistance (R_{SEI}). The semicircle shape is the result of R_{SEI}, charge transfer resistance (R_{CT}), capacitance of SEI layer (Q_{SEI}), and capacitance of double layer (Q_{DL}) in Fig. 5(b). The inclined line in the low-frequency region is related to Warburg diffusion impedance (Z_w) [36]. An SEI layer was not formed at the $Li_4Ti_5O_{12}$ anode because the average operating voltage of $Li_4Ti_5O_{12}$ is 1.5 V. An SEI layer is known to be formed at voltages below 1 V [37].

The Nyquist plots in Fig. 5(a) show that P-$Li_4Ti_{5-x}Cr_xO_{12}$ had a smaller semi-circle than pure-$Li_4Ti_5O_{12}$. The charge-transfer resistances of pure-$Li_4Ti_5O_{12}$, P-$Li_4Ti_{4.97}Cr_{0.03}O_{12}$, P-$Li_4Ti_{4.95}Cr_{0.05}O_{12}$, and P-$Li_4Ti_{4.93}Cr_{0.07}O_{12}$ were 121.1, 49.3, 17.5, and 55.6 Ω, respectively. This can be interpreted to indicate that Cr^{3+} doping and a porous structure can reduce charge-transfer resistance. The charge-transfer resistance is known as the resistance between the electrolyte and the surface of $Li_4Ti_5O_{12}$. P-$Li_4Ti_{4.95}Cr_{0.05}O_{12}$ had a much smaller semi-circle than pure-$Li_4Ti_5O_{12}$, which indicates that P-$Li_4Ti_{4.95}Cr_{0.05}O_{12}$ showed lower charge-transfer resistance than pure-$Li_4Ti_5O_{12}$. Enhanced electrical conductivity by Cr^{3+} doping decreased electron-transfer resistance, and the mesoporous structure increased the diffusivity of lithium ions inside the anode material [38].

However, the charge transfer resistance of P-$Li_4Ti_{4.93}Cr_{0.07}O_{12}$ increased as the Cr^{3+} doping level of $Li_4Ti_5O_{12}$ was increased. It is assumed that extra Cr^{3+} is not completely doped into the lattice of $Li_4Ti_5O_{12}$. Extra Cr^{3+} may be oxidized to Cr_2O_3, which is located on the $Li_4Ti_5O_{12}$ surface, and disturb the diffusion of lithium ions [10,39]. It is very important that the doping level of Cr^{3+} ions should

be optimized.

Cyclic voltammetry analysis was conducted to investigate the electrochemical characteristics of $Li_4Ti_5O_{12}$ and P-$Li_4Ti_{5-x}Cr_xO_{12}$. The operating voltage was between 1.0 and 2.5 V, and the scan-rate was changed from 0.1 to 5 mV/s. Fig. 6(a) and (b) show the various scan-rate cyclic voltammetry (VCV) results of pure-$Li_4Ti_5O_{12}$ and P-$Li_4Ti_{4.95}Cr_{0.05}O_{12}$. Both samples have a pair of redox peaks at around 1.5 V.

Spinel $Li_4Ti_5O_{12}$ is changed to a rock-salt structure by the following reaction [39]:

$$Li_4Ti_5O_{12}+3Li^++3e^- \leftrightarrow Li_7Ti_5O_{12}. \quad (1)$$

$[Li_8]8a[Li_{2.667}Ti_{13.333}]16dO_{32}$ is changed to $[Li_{16}]16c[Li_{2.667}Ti_{13.333}]16dO_{32}$ structure. Lithium is located at 8a (tetrahedral site), and titanium and lithium are located at 16d (octahedral site). The small potential difference of the $Li_4Ti_5O_{12}$ redox peaks indicates lower polarization and better electrochemical properties [40]. A sharp redox peak means that the transfer rate of Li^+ is fast, and a broad peak indicates slow Li^+ transfer [41].

Fig. 6(a) and (b) show that the peaks of P-$Li_4Ti_{4.95}Cr_{0.05}O_{12}$ are sharper than those of pure-$Li_4Ti_5O_{12}$. The transfer rate of Li^+ in P-$Li_4Ti_{4.95}Cr_{0.05}O_{12}$ is faster than that of pure-$Li_4Ti_5O_{12}$, and the doping of Cr^{3+} increased the electrochemical properties. The diffusion coefficient of lithium ions can be calculated by the relation of the peak current and scan rate, and it can be calculated by the Randles-Sevcik equation, which is expressed as [42]

$$I_p = 2.69 * 10^5 * A * n^{\frac{3}{2}} * C_{Li} * D_{Li}^{\frac{1}{2}} * \nu^{\frac{1}{2}} \text{ (at 25 °C)}, \quad (2)$$

where i_p is the peak current (A), A is the surface area of the electrode (cm^2), n is the number of charge transfer electrons (n=1, for Li^+), C_{Li} is the concentration of Li^+ ions ($4.37*10^{-3}$ in $Li_4Ti_5O_{12}$), ν is the scan-rate (mVs^{-1}), and D_{Li} is the diffusion coefficient of lithium (cm^2s^{-1}). The calculated diffusion coefficients of Li^+ from the oxidation and reduction peaks are 2.29×10^{-10} and 1.23×10^{-11} cm^2/s for pure $Li_4Ti_5O_{12}$, and 1.29×10^{-9} and 2.01×10^{-10} cm^2/s for P-$Li_4Ti_{4.95}Cr_{0.05}O_{12}$ as shown in Table 3. These results show that the diffusion coefficients are increased by Cr^{3+} doping, and the charge transfer rate is also increased.

A cycle performance test was conducted to investigate the capacity of $Li_4Ti_5O_{12}$ according to P123 addition and Cr^{3+} doping, and the results are shown in Fig. 7. Rate performance was tested for five cycles at 0.2, 0.5, 1, 2, 5, 10 C-rates as shown in Fig. 7(a). The addition of P123 made pores in $Li_4Ti_5O_{12}$, and the capacities of P-$Li_4Ti_5O_{12}$ were higher than those of pure-$Li_4Ti_5O_{12}$. Cr^{3+} doping enhanced the capacities, and high capacity retention was achieved at

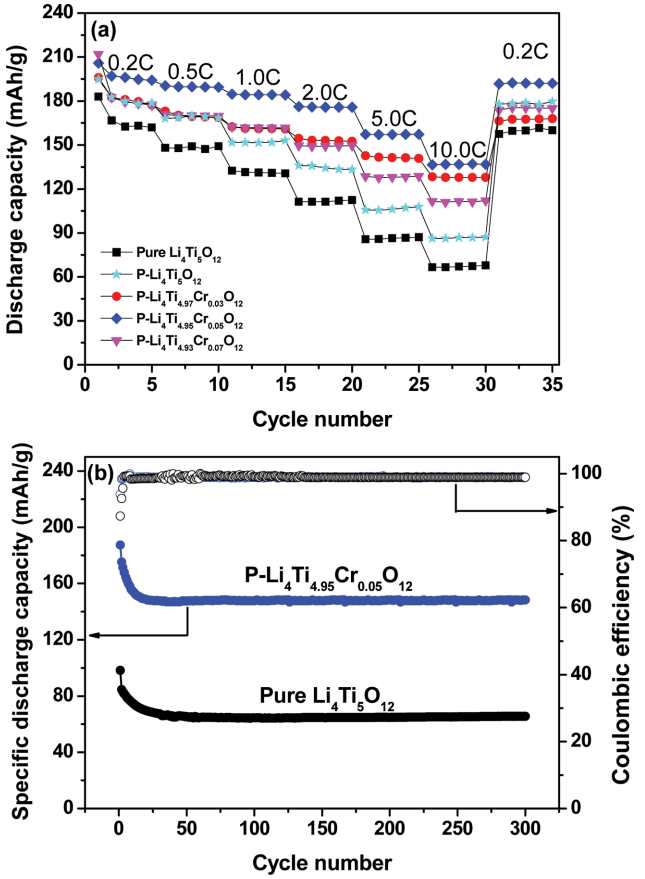

Fig. 7. (a) Rate performance of pure-$Li_4Ti_5O_{12}$ and P-$Li_4Ti_{5-x}Cr_xO_{12}$ ($0\le x\le0.07$) from 0.2 to 10 C-rate at the voltage from 1.0 to 2.5 V and (b) cycling performance and Coulombic efficiency of pure-$Li_4Ti_5O_{12}$ and P-$Li_4Ti_{4.95}Cr_{0.05}O_{12}$ at 10 C-rate from 1.0 to 2.5 V during 300 cycles.

a high C-rate. P-$Li_4Ti_{4.95}Cr_{0.05}O_{12}$ showed excellent capacity properties of 195, 190, 184, 175, 157, and 137 mAh/g at 0.2, 0.5, 1, 2, 5, and 10 C-rates, respectively. This is attributed to the increase of lithium ion diffusion due to P123 addition and the increase of electrical conductivity due to Cr^{3+} doping. P-$Li_4Ti_{4.93}Cr_{0.07}O_{12}$ showed similar capacities as those of P-$Li_4Ti_{4.97}Cr_{0.03}O_{12}$ at low current density. However, the capacities of P-$Li_4Ti_{4.93}Cr_{0.07}O_{12}$ were lower than those of other P-$Li_4Ti_{5-x}Cr_xO_{12}$ at high current density. These results can be explained from the VCV and EIS results because the electrochemical characteristics decreased due to excess Cr^{3+} doping. Cycle performance and Coulombic efficiency were conducted at a 10 C-rate during 300 cycles as shown in Fig. 7(b). Pure-$Li_4Ti_5O_{12}$

Table 3. Diffusion coefficient values of pure $Li_4Ti_5O_{12}$ and P-$Li_4Ti_{5-x}Cr_xO_{12}$ calculated by Randles-Sevcik equation

Samples	Diffusion coefficient (cm^2/s) at cathodic peaks	Diffusion coefficient (cm^2/s) at anodic peaks
Pure $Li_4Ti_5O_{12}$	2.4×10^{-9}	1.35×10^{-10}
P-$Li_4Ti_{4.97}Cr_{0.03}O_{12}$	13.0×10^{-9}	1.99×10^{-9}
P-$Li_4Ti_{4.95}Cr_{0.05}O_{12}$	12.9×10^{-9}	2.01×10^{-9}
P-$Li_4Ti_{4.93}Cr_{0.07}O_{12}$	7.76×10^{-9}	1.05×10^{-9}

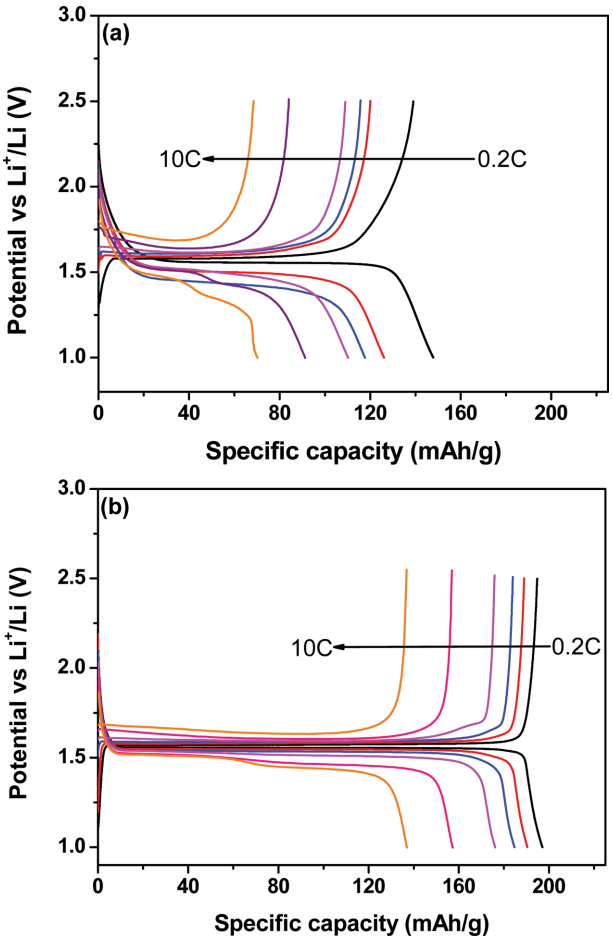

Fig. 8. Charge-discharge profiles of (a) pure-$Li_4Ti_5O_{12}$ and (b) P-$Li_4Ti_{4.95}Cr_{0.05}O_{12}$ from 0.2 to 10 C-rate with the voltage from 1.0 to 2.5 V.

showed about 65 mAh/g, and P-$Li_4Ti_{4.95}Cr_{0.05}O_{12}$ showed about 145 mAh/g.

Fig. 8 shows the charge-discharge profiles of pure-$Li_4Ti_5O_{12}$ and P-$Li_4Ti_{4.95}Cr_{0.05}O_{12}$. A plateau of pure-$Li_4Ti_5O_{12}$ and P-$Li_4Ti_{4.95}Cr_{0.05}O_{12}$ occurred around 1.55 V. Pure-$Li_4Ti_5O_{12}$ showed potential differences of 54, 99, 116, 131, 184, and 293 mV, respectively, and $Li_4Ti_{4.95}Cr_{0.05}O_{12}$ showed those of 17, 34, 56, 79, 129, and 166 mV, respectively, between charge and discharge at 0.2, 0.5, 1, 2, 5, and 10 C-rates, respectively. As the current density became high, the potential difference became large. The potential differences were reduced with P123 addition and Cr^{3+} doping due to the increased Li^+ ion diffusion and electrical conductivity.

CONCLUSIONS

The electrical conductivity of $Li_4Ti_5O_{12}$ was enhanced by Cr^{3+} doping, and Pluronic P123 was used as a dispersant and pore-forming agent for high surface area. Porous-structured Cr^{3+}-doped $Li_4Ti_5O_{12}$ exhibited enhanced electrochemical characteristics, which can be explained as follows. Addition of P123 increased the pore size of $Li_4Ti_5O_{12}$, and the particle size was reduced. The large pore diameter enhanced the diffusion of Li^+ ions. The electron concentration was increased by Cr^{3+} doping, and the electrical conductivity increased. The increase in the Li^+ ion diffusion and the electrical conductivity enhanced the electrochemical characteristics of $Li_4Ti_5O_{12}$. Rate performance tests showed that P-$Li_4Ti_{4.95}Cr_{0.05}O_{12}$ had approximately 99% capacity retention, and its specific capacity was 145 mAh/g at a C-rate of 10 during 300 cycles.

ACKNOWLEDGEMENT

This work was supported by the Technology Development Program (S2719254) funded by the Ministry of SMEs and Startups (MSS, Korea).

REFERENCES

1. D. W. Murphy, R. J. Cava, S. M. Zahurak and A. Santoro, *Solid State Ionics*, **9&10**, 413 (1983).
2. T. Yuan, Z. Tan, C. Ma, J. Yang, Z. F. Ma and S. Zheng, *Adv. Energy Mater.*, **7**, 1601625 (2017).
3. S. C. Hong, H. P. Hong, B. W. Cho and B. K. Na, *Korean J. Chem. Eng.*, **27**, 91 (2010).
4. S. H. Kim, H. Park, S. H. Jee, H. S. Ahn and D. J. Kim, *Korean J. Chem. Eng.*, **26**, 485 (2009).
5. L. Ye, Q. Liang, Y. Lei, X. Yu, C. Han, W. Shen, Z. H. Huang, F. Kang and Q. H. Yang, *J. Power Sources*, **282**, 174 (2015).
6. J. W. Kim, K. E. Lee, K. H. Kim, S. G. Wi, S. H. Lee, S. H. Nam, C. J. Kim, S. O. Kim and B. W. Park, *Carbon*, **114**, 275 (2018).
7. Y. Shi, L. Wen, F. Li and H. M. Cheng, *J. Power Sources*, **196**, 8610 (2011).
8. P. Zhang, Y. Huang, W. Jia, Y. Cai, X. Wang, Y. Guo, D. Jia, Z. Sun and Z. Guo, *Electrochim. Acta*, **201**, 935 (2016).
9. H. Katelen, M. Tuncer, S. Tu, S. Repp, H. Gocmez, R. Thomann, S. Weber and E. Erdem, *J. Mater. Chem. A*, **1**, 9973 (2013).
10. Q. Zhang, Y. Liu, H. Lu, D. Tang, C. Ouyang and L. Zhang, *Electrochim. Acta*, **189**, 147 (2016).
11. C. Lin, M. O. Lai, L. Lu, H. Zhou and Y. Xin, *J. Power Sources*, **244**, 272 (2013).
12. M. Wang, X. Zhang, Y. Wang, L. Cheng and Q. Zhang, *Mater. Sci. Forum*, **960**, 238 (2019).
13. C. Y. Lin and J. G. Duh, *J. Alloys Compd.*, **590**, 3682 (2011).
14. L. Shen, C. Yuan, H. Luo, X. Zhang, K. Xu and Y. Xia, *J. Mater. Chem.*, **20**, 6998 (2010).
15. C. Jiang, M. Ichihara, I. Honma and H. Zhou, *Electrochim. Acta*, **52**, 6470 (2007).
16. D. Liu, C. Ouyang, J. Shu, J. Jiang, Z. Wang and L. Chen, *Phys. Stat. Sol. B*, **243**, 1835 (2006).
17. S. Jamil, R. Yu, Q. Wang, M. Fasehullah, Y. Huang, Z. Yang, X. Yang and X. Wang, *J. Power Sources*, **473**, 228597 (2020).
18. H. Khan and I. K. Swati, *Ind. Eng. Chem. Res.*, **55**, 6619 (2016).
19. G. J. Yang and S. J. Park, *J. Mater. Chem. A*, **8**, 2627 (2020).
20. J. Wolfenstine and J. L. Allen, *J. Power Sources*, **180**, 582 (2008).
21. C. Chen, X. Liu, C. Ai and Y. Wu, *J. Alloys Compd.*, **714**, 71 (2017).
22. D. Qian, Y. Gu, Y. Chen, H. Liu, J. Wang and H. Zhou, *Mater. Lett.*, **238**, 102 (2019).
23. Y. Liu, X. Yan, B. Xu, J. Lan, Y. Yu, X. Yang, Y. Lin and C. Nan, *Chem. Eng. J.*, **361**, 1371 (2019).

24. J. Chen, L. Yang, S. Fang, S. I. Hirano and K. Tachibana, *J. Power Sources*, **200**, 59(2012).
25. H. Wu, S. Chang, X. Liu, G. Wang, D. Cao, Y. Zhang, B. Yang and P. She, *Solid State Ion.*, **232**, 13 (2013).
26. Y. Ge, H. Jiang, K. Fu, C. Zhang, J. Zhu, C. Chem, Y. Lu, Y. Qiu and X. Zhang, *J. Power Sources*, **272**, 860 (2014).
27. S. Saxena and A. Sil, *Mater. Res. Bull.*, **94**, 449 (2017).
28. L. Zhao, Y. Yu, L. Song, M. Ruan, X. Hu and A. Larbot, *Appl. Catal. A-Gen.*, **263**, 171 (2004).
29. I. Hung, Y. Wang, C. F. Huang, Y. S. Fan, Y. J. Han and H. W. Peng, *J. Eur. Ceram. Soc.*, **30**, 2065 (2010).
30. T. Senda and R. C. Bradt, *J. Am. Ceram. Soc.*, **74**, 1296 (1991).
31. Q. Liang, N. Cao, Z. Song, X. Gao, L. Hou and T. Guo, *Electrochim. Acta*, **251**, 407 (2017).
32. F. Li, M. Zeng, J. Li and H. Xu, *Int. J. Electrochem. Sci.*, **10**, 10445 (2015).
33. J. M. Montes, F. G. Cuevas, F. Ternero, R. Astacio, E. S. Caballero and J. Cintas, *Metals*, **7**, 479 (2017).
34. W. Wang, B. Jiang, W. Xiong, Z. Wang and S. Jiao, *Electrochim. Acta*, **114**, 198 (2013).
35. J. H. Jeong, M. S. Kim, Y. H. Kim, K. C. Roh and K. B. Kim, *J. Power Sources*, **336**, 376 (2016).
36. G. Cohn, R. A. Eichel and Y. Ein-Eli, *Phys. Chem. Chem. Phys.*, **15**, 3256 (2013).
37. Y. B. He, M. Liu, Z. D. Huang, B. Zhang, Y. Yu, B. Li, F. Kang and J. K. Kim, *J. Power Sources*, **239**, 269 (2013).
38. Y. Yang, B. Qiao, X. Yang, L. Fang, C. Pan, W. Song, H. Hou and X. Ji, *Adv. Funct. Mater.*, **24**, 4349 (2014).
39. J. G. Kim, M. S. Park, S. M. Hwang, Y. U. Heo, T. Liao, Z. Sun, J. H. Park, K. J. Kim, G. J. Jeong, Y. J. Kim, J. H. Kim and S. X. Dow, *ChemSusChem*, **7**, 1451 (2014).
40. Y. R. Zhu, J. Yuan, M. Zhu, G. Hao, T. F. Yi and Y. Xie, *J. Alloys Compd.*, **646**, 612 (2015).
41. W. Zhu, Z. Zhuang, Y. Yang, R. Zhang, Z. Lin, Y. Lin and Z. Huang, *J. Phys. Chem. Solids*, **93**, 52 (2016).
42. W. Li, M. Chen, J. Jiang, R. Wu, F. Wang, W. Liu, G. Peng and M. Qu, *J. Alloys Compd.*, **637**, 476 (2015).